

1 **Data acquisition by digitising 2D fracture networks and**  
2 **topographic lineaments in GIS: further development and**  
3 **applications**

4 Romesh Palamakumbura<sup>1</sup>, Maarten Krabbendam<sup>1</sup>, Katie Whitbread<sup>1</sup> and Christian Arnhardt<sup>2</sup>

5 <sup>1</sup>British Geological Survey, The Lyell Centre, Research Avenue South, Edinburgh EH14 4AP, UK

6 <sup>2</sup>British Geological Survey, Nicker Hill, Keyworth NG12 5GG

7

8 **Abstract.** Understanding the impact of fracture networks on rock mass properties is an essential part of  
9 a wide range of applications in geosciences, from understanding permeability of groundwater aquifers  
10 and hydrocarbon reservoirs to erodibility properties and slope stability of rock masses for geotechnical  
11 engineering. However, gathering high quality, oriented-fracture datasets in the field can be difficult and  
12 time consuming, for example due to constraints on field work time or access (e.g. cliffs). Therefore, a  
13 method for obtaining accurate, quantitative fracture data from photographs is a significant benefit. In  
14 this paper we describe a method for generating a series of digital fracture traces in GIS-environment, in  
15 which spatial analysis of a fracture network can be carried out. The method is not meant to replace the  
16 gathering of data in the field, but to be used in conjunction, and is well suited where fieldwork time is  
17 limited, or where the section cannot be accessed directly. The basis of the method is the generation of  
18 the vector dataset (shapefile) of a fracture network from a georeferenced photograph of an outcrop in a  
19 GIS environment. From that shapefile, key parameters such as fracture density and orientation can be  
20 calculated. Furthermore, in the GIS-environment more complex spatial calculations and graphical plots  
21 can be carried out such as heat maps of fracture density. Advantages and limitations compared to other  
22 fracture network capture methods are discussed.

23

24

25

26

27

28

29

30

## 31 **1 Introduction**

32 Fractures are the main pathways of fluid flow in rocks and exert a strong influence on rock mass  
33 properties. The characterisation of fracture networks is an essential aspect of various applications in the  
34 Earth sciences, such as understanding the behaviour of fluid flow in groundwater aquifers (Singhal and  
35 Gupta, 2010) and hydrocarbon reservoirs, and the erodibility and slope stability of rock masses (Clarke  
36 and Burbank, 2010; Krabbendam and Glasser, 2011). Fracture network data are essential for assessing  
37 future sites of nuclear waste repositories (Follin *et al.* 2014), predicting rock slope stability (Selby,  
38 1982; Park *et al.* 2005) and understanding rock mass strength for engineering of infrastructure (Hoek  
39 and Brown, 1997; Zhan *et al.* 2017; Ren *et al.* 2017). Thus, fracture network analysis is a critical  
40 component of applied geological characterisation required for ensuring water and energy security,  
41 supporting infrastructure development, and protecting human health, which are identified as key  
42 Sustainable Development Goals (Schrodt *et al.* 2019).

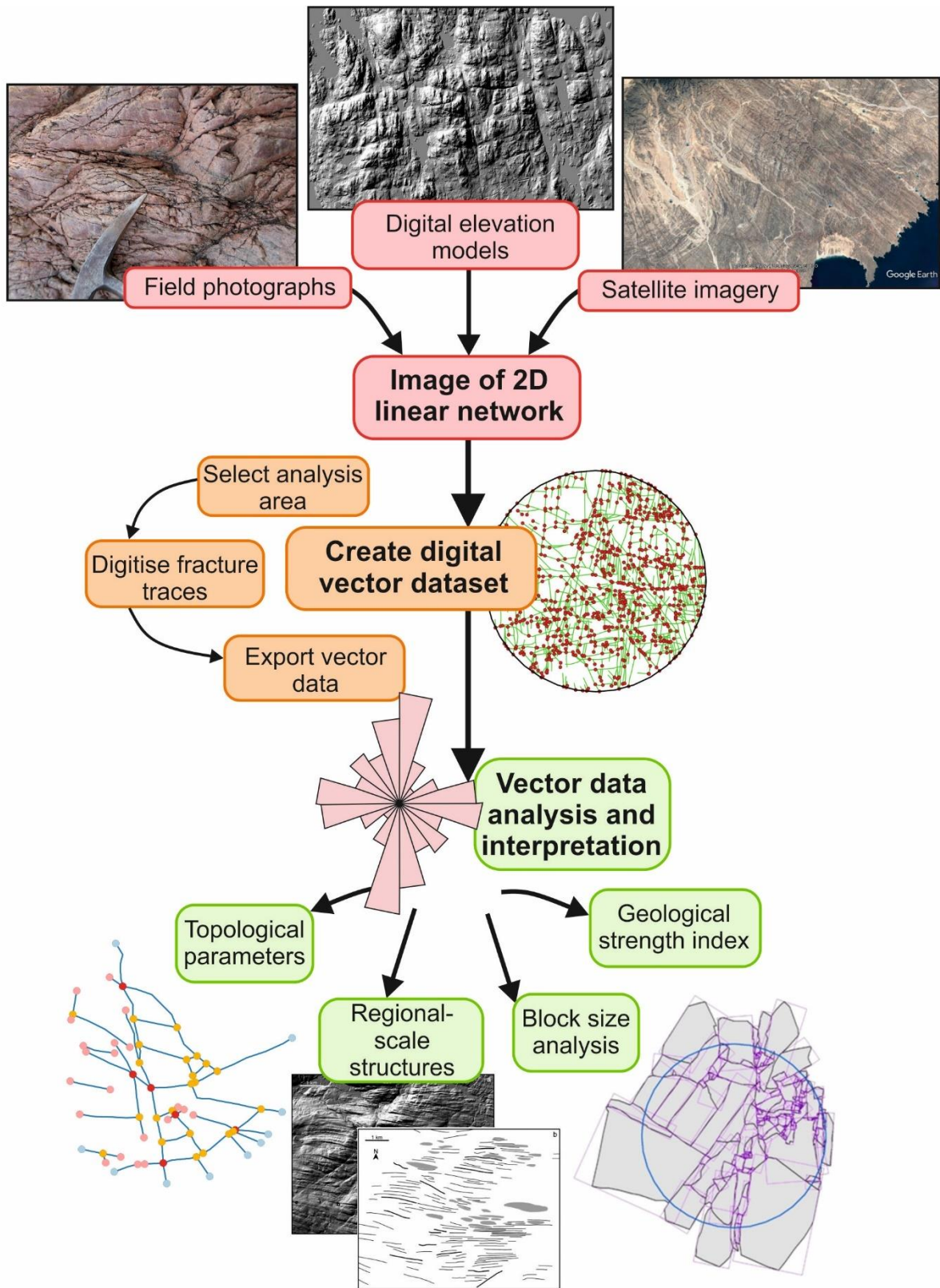
43 To characterise fracture networks, a range of fracture network parameters need to be acquired, including  
44 the fracture density, connectivity, and orientations (e.g. Singhal and Gupta, 2010). These properties can  
45 be highly spatially variable over a range of scales, which cannot be accurately predicted (Long *et al.*  
46 1987). The comprehensive capture of observational data is typically required to characterise fracture  
47 network variability over large areas. Due to the limited distribution of suitable rock exposures in many  
48 settings, understanding the spatial variability of fracture network parameters at regional scales requires  
49 sampling at multiple sites (e.g. McCaffrey *et al.* 2020). Practical constraints on data collection are  
50 therefore critical factors. Constraints on the number of sites that can be analysed in a given study  
51 increases uncertainty in estimations of fracture properties of the wider rock mass. This uncertainty limits  
52 the scales at which analyses can be reasonably applied.

53 The need for efficient and robust methods for quantitative capture of fracture data is well recognised,  
54 and methods using statistically-based observational techniques (Mauldon *et al.* 2001), and systematic  
55 regional sampling (e.g. Watkins *et al.* 2015a) have been proposed previously. We build on previous  
56 developments in fracture sampling by focusing on a method for digital data capture from 2D outcrop  
57 images.

58 Advanced 3D methods for outcrop imaging and fracture analysis are now available (Tavani *et al.* 2016;  
59 Bisdom *et al.* 2017), but limited access to necessary hardware, software and training technology may  
60 limit the wider adoption of these high-cost techniques in many applied research contexts. In contrast,  
61 the ready availability of digital cameras and suitable open-source software means that the 2D digital  
62 capture method has potential for wider adoption across applied geoscience fields where traditional, low-  
63 cost 1D and analogue sampling methods are still widely used (Siddique *et al.* 2015; Panthee *et al.* 2016).  
64 Systematic 2D digital capture has particular relevance for studies (1) where large datasets are required  
65 from multiple sites, (2) where advanced outcrop scanning or unmanned aerial vehicle (UAV) systems

66 are not available or are impractical to use; (3) where historic images (such as from quarries, canal  
67 excavations or road cuttings) provide a valuable data source, or (4) for multi-scalar analysis using micro  
68 (e.g. thin section) to macro (e.g. satellite) scale images.

69 Here we describe good practice in the use of a low-cost 2D digital method for efficient capture and  
70 visualisation of a range of fracture parameters and illustrate how these methods can be used across a  
71 range of applied geoscience fields (Figure 1). Although the method has been used before (Krabbendam  
72 and Bradwell, 2014; Watkins *et al.* 2015a; Krabbendam *et al.* 2016; Healy *et al.* 2017) no  
73 comprehensive description of the method has been published.



74

75 **Figure 1:** Flowchart providing an overview of the 2D digital capture method y used for digitising linear features,  
 76 from preparing an image, digitising the features to output of data. Digital elevation model examples are  
 77 taken from Next map © in Scotland, and the satellite image of Oman example is taken from Google Earth  
 78 ©.

## 79 2. Summary of fracture data capture methods

80 Understanding the effect of a fracture network on the properties of a rock mass requires acquisition of  
81 various parameters such as length, orientations, density and spacing (Singhal and Gupta, 2010).  
82 Network topology is used to understand how connected a fracture network is and can be characterised  
83 by derived parameters such as fracture connectivity, percolation potential and clustering (Manzocchi,  
84 2002; Sanderson and Nixon, 2015). Finally, fracture aperture, fill and paragenesis history provide an  
85 important understanding of the fracture network history, fluid flow and fracture strength (Carlsson, and  
86 Olsson, 1976; Laubach *et al.* 2019).

87 Fracture networks can be characterised in different dimensions using a number of approaches. 1D  
88 approaches include outcrop-based scanline surveys and (by necessity) borehole fracture analysis,  
89 typically represented by the number of fractures per unit length, i.e. frequency. 1D approaches are  
90 relatively rapid, but do not directly constrain parameters such as fracture length and connectivity. If  
91 the fracture network is anisotropic, which is commonly the case, the characterisation is biased by the  
92 orientation of the scanline or the borehole ('orientation bias'; Singhal and Gupta, 2010; Zeeb *et al.*  
93 2013; Watkins *et al.* 2015b).

94 In 2D fracture network analysis, a circular sampling window is commonly used (Davies *et al.*, 2011;  
95 Rohrbaugh *et al.* 2002; Watkins *et al.* 2015a). In the field, a circular 'chalk line' is drawn on an outcrop,  
96 within which the fractures and key geometries are captured. Connectivity within the fracture network  
97 can be parameterized by characterising the different types of fracture terminations and intersections,  
98 which can be used to understand fluid percolation potential (e.g. Manzocchi, 2002). Full field-based  
99 capture is very time consuming, particularly when data from multiple sites are required, and may be  
100 impractical or impossible for some outcrops, such as quarries, cliffs and coastal platforms. Time  
101 constraints normally mean that field-based methods are also limited in their scale of application, with  
102 sampling window diameters of 1 – 2 m being commonly used (e.g. Watkins *et al.* 2015a; Procter and  
103 Sanderson, 2018). This limitation means that spatial variability in fracture properties at scales greater  
104 than 5-10 m are typically not captured.

105 To overcome the time-constraints of the full 2D window approach, a circular scanline method was  
106 developed (Mauldon *et al.* 2001), in which only those fractures that intersect a particular circular  
107 scanline are captured; in a sense it is similar to the 1D approach. The circular scanline analysis is more  
108 rapid than the full 2D circular window analysis and has less length and orientation bias compared to 1D  
109 methods (Mauldon *et al.* 2001). The circular scanline method can be used to calculate proxies for (but  
110 does not directly measure) fracture density and length based on the ratio of the types of trace intersection  
111 (Mauldon *et al.* 2001), however if other parameters are needed further field work would be required.

112 Ideally, for any application, a full 3D characterisation of the rock mass is achieved. However, true 3D  
113 characterisation of a rock mass is currently only possible using CT scanning, and is restricted to very

114 small samples (Voorn *et al.* 2015). High resolution ‘3D’ images of outcrop surfaces (more like ‘2.5D’)  
115 can be captured by laser scanning, which can be ground based or acquired by UAV (e.g. Bisdorn *et al.*  
116 2017; Gao *et al.* 2017; Wüstefeld *et al.* 2018). From the laser scans, 3D images of the outcrop surface  
117 (3D ‘virtual outcrop’) can be generated using techniques such as structure from motion (SfM)  
118 photogrammetry (Vasuki *et al.* 2014). These can provide additional information on fracture orientation  
119 through the use of advanced image analysis techniques (Wüstefeld *et al.* 2018). These methods have  
120 been used for advanced fracture network analysis and modelling for applications related to fluid flow,  
121 gas migration and engineering/construction (e.g. Bisdorn *et al.* 2017; Menegoni *et al.* 2019; Strijker *et*  
122 *al.* 2012; Tavani *et al.* 2016). These 3D scanning techniques require sophisticated hardware, proprietary  
123 software and training that potentially limits their applicability. In addition, there are practical limitations  
124 at sites, such as access and restrictions on the use of UAVs, that may further limit their use (e.g. Senger  
125 *et al.* 2015).

126 The 2D fracture network can be captured in the field as well as from image tracing (e.g. Watkins *et al.*  
127 2015a). Digital 2D data capture can be applied to photographs of an outcrop or thin section, aerial  
128 photographs, or satellite imagery. 2D digital data capture methods can thus be used at a great range of  
129 scales, permit data acquisition from inaccessible sites, and provides a reproducible approach from which  
130 a digital dataset suitable for numerical and statistical analysis can be readily derived. The 2D digital  
131 capture typically relies on GIS-type functions for the visualisation and analysis of images, and uses  
132 standard GIS tools. More sophisticated analysis can be carried out using software applications such as  
133 proprietary DigiFract which is based on customised QGIS functions (Hardebol and Bertotti, 2012), the  
134 open-source tool FracPac for Matlab (Healy *et al.* 2017) and NetworkGT for QGIS (Nyberg *et al.* 2018).  
135 These tools provide enhanced functions for efficient capture of data from images and advance data  
136 analysis, but are targeted for application in structural geology research contexts.

137 In its basic form, the 2D digital data capture method requires only a digital camera, a measuring stick  
138 and access to GIS, such as open-source QGIS. The low-cost nature of the method means that this is  
139 potentially a powerful tool for enhancing geological investigations across a range of applied studies,  
140 such as engineering geology and hydrogeology. We comprehensively describe good practice for 2D  
141 digital fracture capture and analysis. In particular we focus on the practical aspects of image capture,  
142 preparation and analysis using QGIS and other open-source tools and plugins. Four case studies are  
143 presented to illustrate a number of practical applications. We demonstrate some simple fracture analysis  
144 tools that can be applied to the captured data. Finally, we evaluate the benefits and drawbacks of 2D  
145 digital data capture compared to other approaches for capturing fracture data.

146

147

148

### 149 **3 Digital 2D fracture analysis method**

150 The 2D digital capture method in essence captures a set of digital traces (vectors) of a 2D linear feature  
151 network in a GIS project from a georeferenced image. Here, we use open source GIS software (QGIS),  
152 making the method accessible to all potential users. A number of open tools within QGIS can be used  
153 for more advanced analysis of the digitised fracture network.

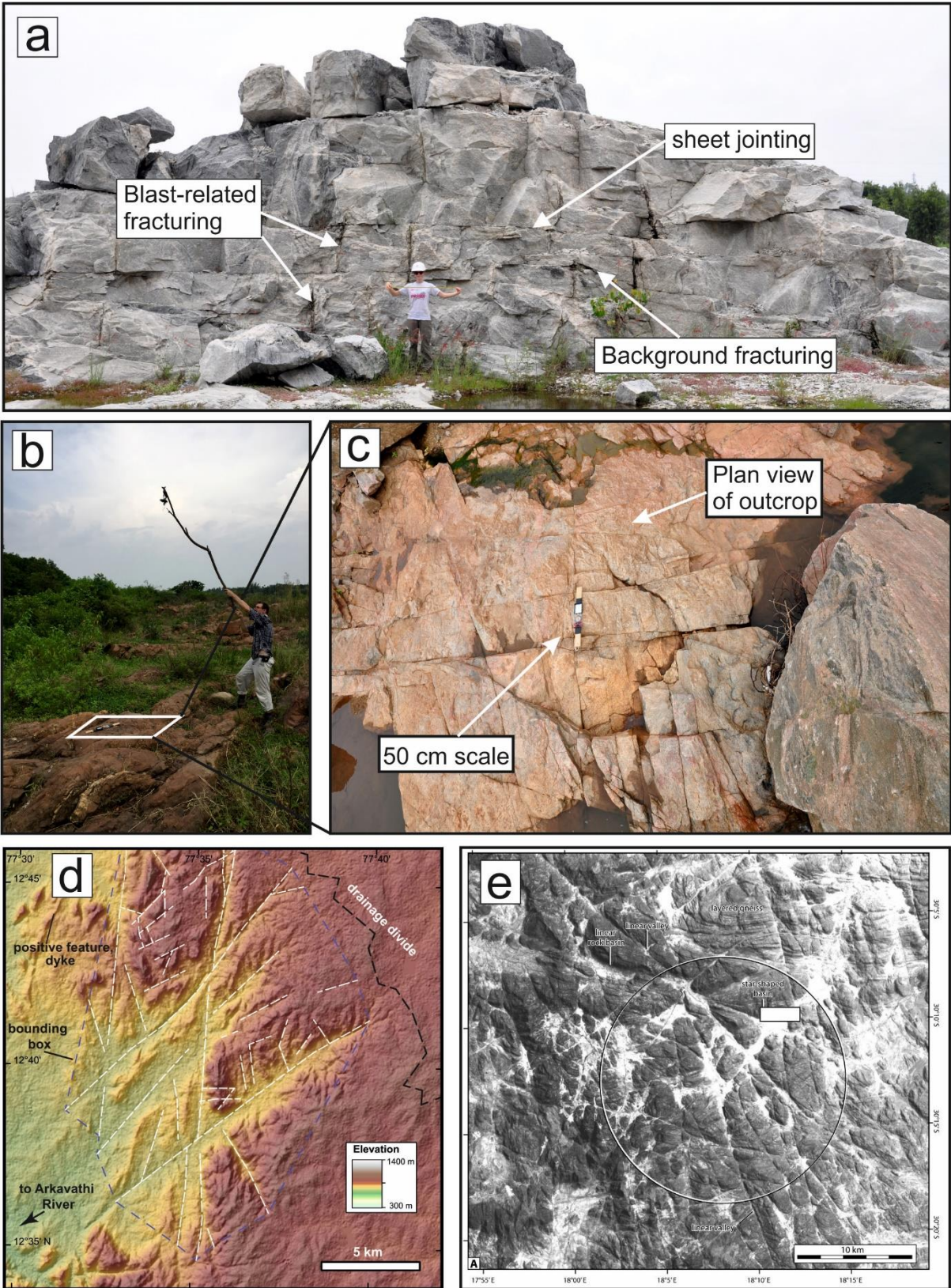
#### 154 **3.1 Outcrop selection**

155 A suitable outcrop for digital fracture analysis must be first selected. The outcrops selected will depend  
156 on the nature of the study being undertaken and the type of fracture network parameters required  
157 (Watkins *et al.* 2015a). It is important to consider whether the outcrop is representative of the rock mass  
158 as a whole or whether multiple sites would better represent the diversity of fracture characteristics.  
159 Outcrop selection has significant implications on the final results, i.e. whether the outcrop is a proxy  
160 for wider-scale fracture network characteristics at depth or if it is the outcrop itself that is being studied  
161 in isolation (Laubach et al 2019; Ukar et al 2019).

162

#### 163 **3.2 Outcrop image preparation**

164 The first step is to capture or prepare a suitable photograph or image of the outcrop to be analysed. The  
165 image can be a photograph of a fracture network at outcrop of various scales from centimetres to 10s  
166 of metres. It is important that the fractures can be clearly identified in the photograph, and that not too  
167 much of the image is occupied by vegetation or broken ground (Figure 2a). It is important to include  
168 an accurate and clearly identifiable scale; a strip of plywood with duct tape works very well. However,  
169 in some dangerous outcrops (e.g. working quarries) this may be impractical and quarry machinery or  
170 other features of known dimensions may be used as a scale in the photograph. This also applies to  
171 historic photographs. The photograph should be taken at right angles (or as much as possible) to the  
172 outcrop to minimise the issues created by a distortion of the image. The camera should have a focal  
173 length of 35mm (analogue 35 mm equivalent) or longer, to prevent further distortion. Horizontal  
174 outcrops should be photographed vertically to again minimise the distortion of the fractures. Mounting  
175 the camera on a stick is useful to increase the distance and capture a larger field of view (Figure 2b, c);  
176 drones also be used. For horizontal outcrops it is convenient to orient the measuring stick accurately to  
177 the north, using a compass (Figure 2c), this will help in capturing the correct orientations of the  
178 fractures.



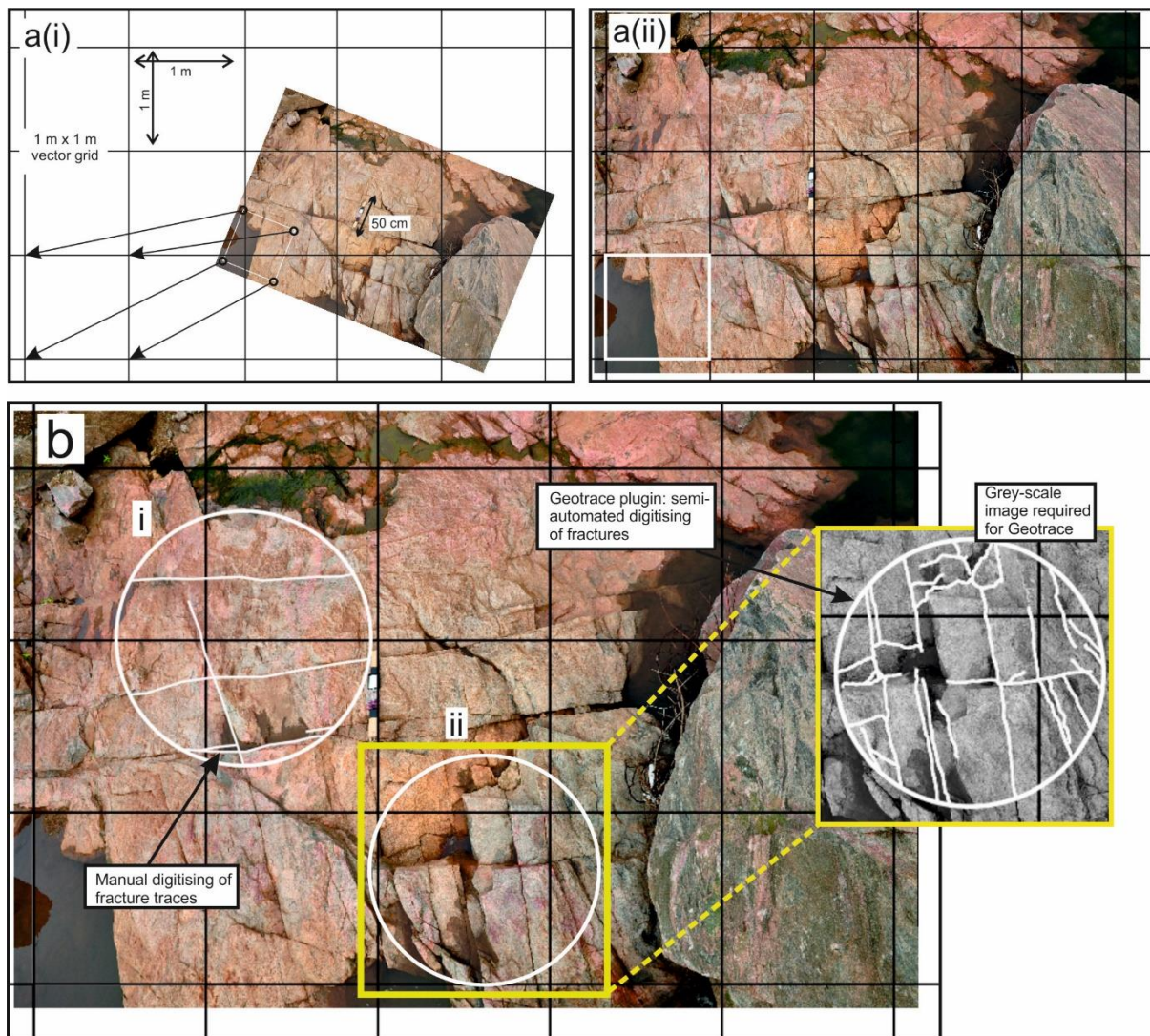
179

180 **Figure 2:** Examples of photographs and DEM images that can be used for digitising 2D linear features, including:  
 181 (a-c) photographs of fracture networks of various scale from southern India and improvised methods for taking  
 182 photographs parallel to the outcrop; (d) a DEM image from southern India of larger kilometre scale features that

183 could also be digitised; and (e) an aerial photography from Namibia (adapted from Krabbendam and Bradwell,  
184 2014).

### 185 3.3 Georeferencing the images

186 To aid robust georeferencing, the photograph needs to have a square of known size (e.g. 1 x 1 m)  
187 embedded in it. This is done by importing the photograph into a graphics software package (such as  
188 Inkscape), and drawing a square based on the scale included in the original photograph (Figure 3). The  
189 photograph with the embedded 1 x 1 m square is then imported into a new GIS project file. The GIS  
190 project file needs a projection in metres; we recommend a Mercator projection, (such as EPSG:3857).  
191 Within the GIS project, a ‘vector grid’ (fishnet grid) is created, with a grid extent that is larger than the  
192 imported photograph and with a vertical and horizontal spacing of 1.0 m. Finally, the square on the  
193 photograph is georeferenced to a square on the fishnet grid (Figure 3a).



194

195 **Figure 3:** Images showing (a (i-ii)) how to georeference an image to a fishnet grid (black) from a square of a  
196 known scale (white); and (b) the tools available for digitising fractures in QGIS, including (i) a fully manual  
197 method; and (ii) a semi-automatic method such as Geotrace.

### 198 **3.4 Using DEM, satellite and air photo images**

199 DEMs (Digital Elevation Models) (and their hill-shaded derivatives), satellite images and  
200 (orthorectified) aerial photographs commonly show good topographic lineaments that likely represent  
201 fracture zones, or master joints (Fig. 2d,e). Such imagery is commonly already georeferenced and can  
202 be used without further preparation. It should be noted however that aerial photographs, DEMs and  
203 satellite images do not directly show fracture traces, rather they show the topographic expression of  
204 these. Thus, fracture density is likely to be underestimated, because fractures without topographic  
205 expression will not be captured. Figure 2d is an example of a DEM image from southern India showing  
206 kilometre-scale 2D topographic lineaments: in some parts lineaments are well developed, in other parts  
207 fracture zones have no expression and presumably occur beneath a continuous layer of regolith.  
208 Furthermore, such imagery is limited by the on-ground resolution, so that smaller-scale (smaller  
209 aperture) fractures may not appear. Hill-shade DEM images, as well as satellite imagery and aerial  
210 photographs have the problem of bias by a particular direction of illumination, so that lineaments of  
211 one orientation may be clearer than others. For DEMs, hill-shades derivatives with different  
212 illumination direction can be made; for satellite imagery, sometimes imagery taken at a different time  
213 of day are available. Hence, for DEM-scale interpretations it is important to take a multi-data type  
214 approach (e.g. DEMs and satellite images) to guide digitisation, similar to that of Pless (2012).

215

### 216 **3.5 Data capture**

#### 217 **3.5.1 Create analysis window**

218 As a first step, create a polygon shapefile and digitise the area (window) to be analysed. An example is  
219 shown in Figure 3b as two circular windows (in white), digitised onto a photograph in GIS. It is  
220 important to create a different id number for each shape that includes details of the photograph or image  
221 that is being digitised. Multiple windows can be used on the same imagine, in particular if the image  
222 shows spatial variability of the fracture network.

#### 223 **3.5.2 Digitise linear features**

224 This step aims to create a series of digital line traces from the georeferenced image. Create a new line  
225 shapefile in the GIS project to hold the linear trace data. The shapefile needs to include an id column in  
226 the attribute table so that the linear traces can be associated with its specific window polygon. Two  
227 methods can be used to create digital traces of the linear features. Firstly, the individual features can be  
228 digitised manually in the GIS project, using the “add line features” tool. Alternatively, the plugin tool

229 “GeoTrace” can be used to semi-automate the digitising process. The GeoTrace plugin tool in QGIS  
230 allows one to click on the start and end of each fracture and GeoTrace creates a line vector between  
231 these points. For this method the photograph must be in grey scale, because the plugin follows the linear  
232 feature based on low raster values and requires a sharp contrast between the feature and the background.  
233 When digitising fracture traces it is important to only digitise in one orientation: if a feature has multiple  
234 orientations along its length then multiple line segments should be digitised. Figure 3b is an example  
235 of both (i) manual digitisation and (ii) semi-automated digitisation with GeoTrace. In both the manual  
236 and semi-automated methods, connecting fractures should be properly snapped against each other, and  
237 to the surrounding circular window.

238 In quarries or excavated sections, it can be challenging to distinguish natural joints from those arising  
239 from quarrying processes, such as blast damage or drilling related fractures. Using field observations,  
240 blast damage can be separated from natural joints (Figure 2a). Joints arising from blast damage can  
241 easily be distinguished from natural joints as they do not fit with the overall fracture pattern, and are  
242 generally surrounded by small radiating fractures.

### 243 **3.6 Data output and further analysis**

244 The final step is to generate basic parameters and calculate dimensions from the digital traces of the  
245 linear features. There are a number of different ways that the vector data can be processed, which  
246 include: 1) using the field calculator in QGIS; 2) as an exported spreadsheet; or 3) using a programming  
247 language such as Python or *R* to make calculations from the spreadsheet or directly from the shapefile.

248 Primary parameters such length and orientation of individual fracture traces can be calculated within  
249 the field calculator in the QGIS attribute table. The area of the circular window can also be calculated  
250 in the attribute table using the field calculator. For further processing, the attribute table containing the  
251 primary fracture data (length, orientation and reference to the circular window) needs to be exported as  
252 a spreadsheet, e.g. in CSV format. Fracture density ( $D$ ) within the circular window can now be  
253 calculated using total length of fractures ( $\Sigma L$ ) within the area of the circular window ( $A$ ), following  
254 Singhal & Gupta, (1999):

$$255 \quad D = \Sigma L / A \quad (\text{in m}^{-1}) \quad (1)$$

256 Fracture spacing ( $S$ ) can be easily derived, as this is the reciprocal of fracture density, and is given by  
257 (Singhal & Gupta, 1999):

$$258 \quad S = A / \Sigma L \quad (\text{in m}). \quad (2)$$

259 Fracture intersections (points) within the fracture network, important to constrain connectivity  
260 (Manzocchi, 2002) can be created as a separate point shapefile with the ‘line intersection’ tool. The  
261 digitised fracture traces can also be used to derive block size parameters, using the ‘polygonise’ tool to

262 convert the line vectors into polygons. As before, parameters such as area can be derived using the field  
263 calculator in the attribute table and exported as a spreadsheet.

#### 264 **4 Case studies**

265 To illustrate the use of systematic 2D digital fracture analysis methods for applied geoscience  
266 investigation we present a number of case studies to highlight a range of geoscience applications and  
267 illustrate key benefits, including: (1) Rapid data collection to support regional hydrogeological  
268 assessment (India); (2) Enabling quantitative, rather than typical qualitative, assessment of key  
269 parameters for engineering Rock Mass Strength evaluation (India); (3) Analysing catchment-scale  
270 variability in sediment source characteristics for applied geomorphic studies in erosional terrains  
271 (Scotland), and; (4) Fracture network analysis from historical images for sites where modern exposures  
272 are unavailable (Sweden).

#### 273 **4.1 Understanding fracture connectivity and permeability, southern India**

274 Characterisation of fracture networks is essential to understand local and regional-scale aquifer  
275 properties such as connectivity and permeability, in particular in fractured ‘hard-rock’ aquifers, where  
276 fractures are the primary water stores and pathways (e.g. Stober and Bucher, 2007; Singhal and Gupta  
277 2010; Guihéneuf *et al.* 2014). An example is given here of the Peninsular Gneiss in the Cauvery  
278 Catchment in southern India. The groundwater properties of the Cauvery Catchment have been an area  
279 of ongoing research (Maréchal *et al.* 2006, Perrin *et al.* 2011, Collins *et al.* 2020) as the spatial and  
280 temporal variability of groundwater availability has profound implications for the sustainability of  
281 irrigation and hence food security. Two contrasting basement fracture networks can be identified  
282 (Figure 4a-b): firstly, massive gneiss with few fractures, dominated by a widely spaced ‘background  
283 jointing’ and sheeting joints close to the surface; and secondly ‘fracture zones’ that are characterised by  
284 a very dense fracture network. Data were collected during a very short, reconnaissance-type fieldwork.

285 Length-weighted rose plots show the variation in orientation of fractures (in a vertical section) in the  
286 two identified domains (Figure 4c, d). In the massive gneiss the fractures are generally orientated sub-  
287 horizontally, with several short connecting vertical fractures. In contrast, fractures in the fracture zones  
288 are generally orientated sub-vertically with short connecting sub-horizontal fractures. The fracture  
289 density in the fracture zones is an order of magnitude higher than in the massive gneiss (Table 1). Using  
290 NetworkGT (Nyberg *et al.* 2018), the fracture branches and nodes (intersections and fracture trace end-  
291 points) were characterised based on the topology of the branch intersections (Manzocchi, 2002;  
292 Sanderson and Nixon, 2015). The massive gneiss is dominated by I-type nodes, whereas the fracture  
293 zones predominantly contain a combination of Y- and X-type nodes (Figure 4a-b; for node types see  
294 Figure 4g) (Table 1). Heat maps of intersection clustering illustrate the higher fracture connectivity  
295 within the fracture zones. To quantify the connectivity, the connections per line and dimensionless  
296 intensity (a representation of intensity that uses average fracture length) were calculated (following

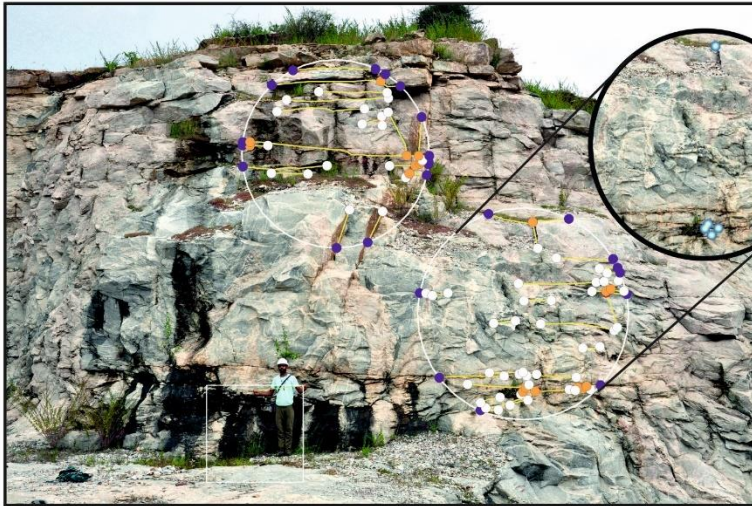
297 Sanderson and Nixon, 2015), (Table 1; Figure 4h). The number of connected (X- and Y) nodes per  
 298 fracture line length is an indication of the percolation potential of a fracture network (Sanderson and  
 299 Nixon, 2018). The fracture zones have the highest connections per line length and dimensionless  
 300 intensity, indicating they have the highest potential connectivity. In contrast, the background gneiss has  
 301 the lowest connections per line and intensity, suggesting a relatively low potential connectivity. The  
 302 coefficient of variation (Cv) was calculated by dividing the standard deviation of the fracture spacing  
 303 by the mean fracture spacing (Gillespie *et al.* 1999; Watkins *et al.* 2015b) and was used to quantify the  
 304 how clustered a fracture network is (Table 1) (Odling *et al.* 1999). The Cv ratios show that the massive  
 305 gneiss generally has regularly-spaced fractures, while the fractures in the fracture zones are highly  
 306 clustered (Table 1, Figure 4h).

307

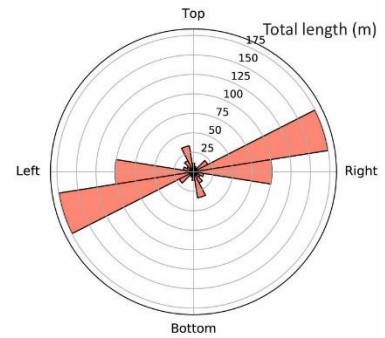
Rock type	Area (m <sup>2</sup> )	Mean length (m)	2D density (m <sup>-2</sup> )	I	U	X	Y	Dimensionless intensity	Connections per line	Coefficient of variation (Cv)
Massive gneiss	15.0	0.6	1.4	41.0	10.0	1.0	11.0	0.8	0.9	0.2
Massive gneiss	11.9	1.0	1.9	19.0	15.0	0.0	10.0	1.9	1.4	0.6
Massive gneiss	26.8	0.5	3.9	136.0	32.0	18.0	157.0	2.0	2.4	0.8
Massive gneiss	8.5	0.3	8.8	130.0	40.0	38.0	204.0	2.7	2.9	1.3
Massive gneiss	137.8	2.9	0.7	21.0	10.0	6.0	23.0	1.9	2.6	0.9
Massive gneiss	359.4	11.9	0.2	5.0	4.0	1.0	1.0	2.0	1.3	1.8
Massive gneiss	31.1	5.3	0.7	3.0	5.0	0.0	0.0	3.6	0.0	1.1
Massive gneiss	13.3	2.1	0.9	2.0	8.0	0.0	2.0	1.9	2.0	0.5
Massive gneiss	10.5	1.9	0.9	2.0	5.0	2.0	1.0	1.7	4.0	0.7
Massive gneiss	119.6	2.1	0.8	41.0	12.0	4.0	27.0	1.6	1.8	0.4
Massive gneiss	95.4	2.3	1.0	29.0	19.0	5.0	30.0	2.4	2.4	0.5
Fracture zone	4.6	0.2	17.8	157.0	61.0	121.0	517.0	3.3	3.8	1.4
Fracture zone	45.2	0.9	3.9	139.0	38.0	45.0	174.0	3.4	2.8	1.4
Fracture zone	38.5	1.7	1.6	139.0	38.0	45.0	174.0	2.6	2.8	1.3
Fracture zone	81.6	2.6	1.1	23.0	16.0	6.0	25.0	2.8	2.6	1.2
Fracture zone	9.2	1.5	1.4	4.0	6.0	0.0	6.0	2.1	2.4	0.7

308 **Table 1:** Summary fracture network statistics from the Peninsular Gneiss in the Cauvery Catchment,  
 309 southern India.

(a) Digital fracture traces on massive gneiss

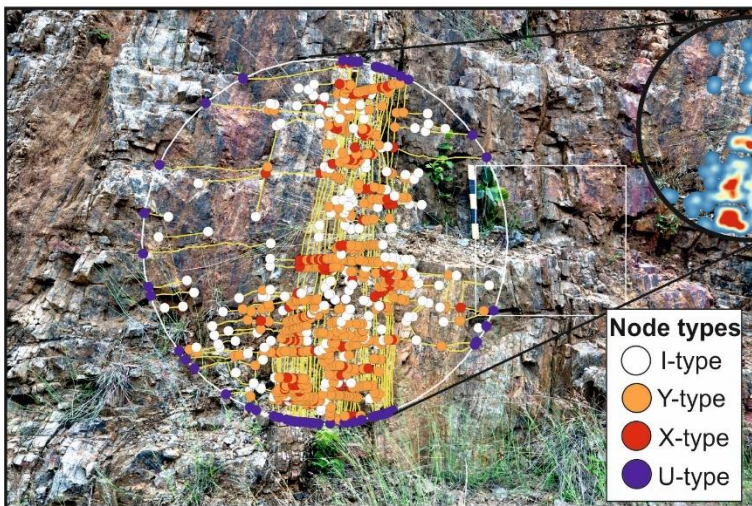


(c) Heat map of intersection density

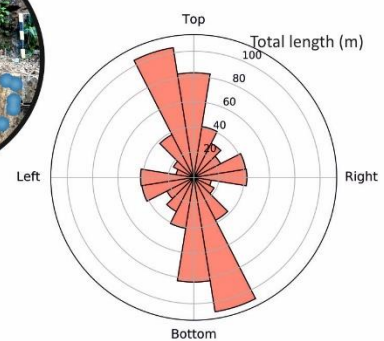


(e) Rose plot of fractures in background gneiss (n=176)

(b) Digital fracture traces from fracture zone

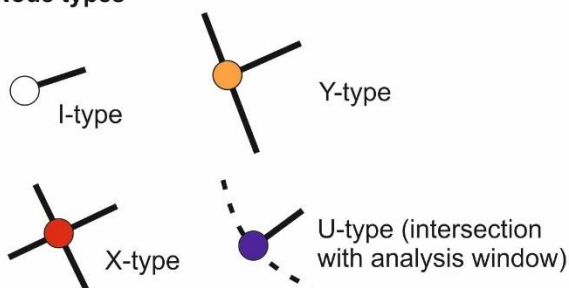


(d) Heat map of intersection density

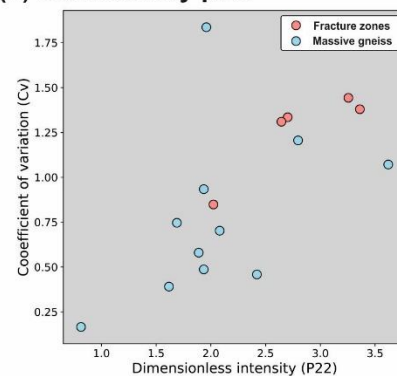


(f) Rose plot of fractures from fracture and shear zones (n=1104)

(g) Node types



(h) Connectivity plot



310

311 **Figure 4:** Fracture analysis from the Peninsular Gneiss, South India, including: field photographs with digitised  
 312 fracture branches and intersection types on (a) a massive gneiss example; and (b) from a fracture zone; (c-  
 313 d) heat maps illustrate variations in fracture intersection density (massive gneiss: 0-5 nodes/m<sup>2</sup> and  
 314 fracture zones: 0-18 nodes/m<sup>2</sup>); (e-f) length-weighted rose plots showing the variation in orientation of  
 315 fractures traces in the background gneiss and fracture zones; (g) a schematic illustration of the various

316 types of fracture connections (as defined by Manzocchi, 2002); (h) a plot of connections per line against  
317 dimensionless intensity (defined by Sanderson and Nixon, 2015) to show variations in connectivity.

318

319 At the near-surface, the Peninsular Gneiss has a bimodal fracture density distribution with fracture  
320 zones with high fracture density that make up a relatively small proportion of the bedrock, and the  
321 majority of the crystalline basement containing a low-density fracture pattern. Derived connectivity  
322 parameters indicate the highest potential permeability is found in the fracture zones, whereas the  
323 background gneiss has significantly lower potential permeability.

324 In this case study, field time was limited and the 2D digital method provided a rapid and flexible way  
325 of gathering fracture network data. It was possible to carry out a reconnaissance survey covering an  
326 area over 30,000 km<sup>2</sup> and then retrospectively select the most suitable sites for fracture analysis. Key  
327 fracture parameters such as fracture length, orientation and density, which impacts on aquifer  
328 characteristics such as connectivity and permeability across the Peninsular Gneiss in the Cauvery River  
329 catchment, were then calculated and used to constrain local and regional-scale groundwater models  
330 (Collins *et al.* 2020).

#### 331 **4.2 Rock mass strength estimates (Geological Strength Index)**

332 Structural discontinuities are an important control on the engineering behaviour of a rock mass (Barton  
333 *et al.* 1974; Müller, 1974; Hoek 1983, Hoek & Brown 1997). Slopes, foundations and underground  
334 excavations in hard rock can be strongly affected by the presence of discontinuities; for example, the  
335 intersection of structural features can lead to falling and sliding of blocks or wedges from the surface.

336

337 In the last decade, rock mass classification systems have been applied extensively in engineering design  
338 and construction (Liu, 2007). The Geological Strength Index (GSI) system provides a numerical  
339 representation of the overall geotechnical properties of a rock mass, which is estimated using a standard  
340 matrix chart and field observations of (a) the ‘blockiness’ of a rock mass and (b) the surface conditions  
341 of any discontinuities. The GSI Index is based upon an assessment of the lithology, structure and  
342 condition of discontinuity surfaces in the rock mass and it is estimated from visual examination of the  
343 rock mass exposed in surface excavations such as roadcuts, in tunnel faces and in borehole core  
344 (Marinos and Hoek, 2000). Both the ‘blockiness’ and surface conditions, however, are determined in a  
345 qualitative and descriptive manner, which is subjective and dependent on the interpreter. Sönmez and  
346 Ulusay (1999; 2002) suggested that the ‘blockiness’ or Structure Rating should be quantified by using  
347 the Volumetric Joint (fracture) Count ( $J_v$ , in m<sup>-1</sup>). This parameter is defined as the sum of the number  
348 of joints per meter for each joint set present (Sönmez & Ulusay, 1999):

349

350 
$$Jv = \frac{1}{s_1} + \frac{1}{s_2} + \dots + \frac{1}{s_n} \quad (3)$$

351

352 where  $S$  is the spacing of the joints in a set and  $n$  is the number of joint sets. The 2D fracture digitisation  
353 method can clearly be applied to determine an accurate representation of  $Jv$  from an image.

354

355 The procedure for quantifying rock mass strength parameters in jointed rocks is illustrated using  
356 massive and fractured gneiss exposures in India (Figure 4). Using the qualitative method (Hoek, 1983)  
357 the massive gneiss, with ‘good’ fracture surfaces, has a GSI index of 70-85 whereas the fractured gneiss,  
358 with ‘fair’ fracture surfaces, has a GSI index of 30-45. To quantify this, the modified GSI methodology  
359 after Sönmez & Ulusay (1999) is used. In this example, the massive gneiss has a horizontal joint spacing  
360 of 0.81 m (J1) and a vertical joint spacing of 6.19 m (J2). The fractured gneiss has a horizontal joint  
361 spacing of 0.17 m (J1) and a vertical joint spacing of 0.08 m (J2). Applying equation 3, this gives a  $Jv$   
362 value of 1.4 for the massive gneiss and 17.7 for the fractured gneiss. Based on similar estimates of  
363 roughness (5), weathering (3) and infill (6) the fracture surface condition rating (SCR) is 14 in both the  
364 massive gneiss and the fracture zones. Finally, the GSI values for the massive gneiss was calculated as  
365 *c.* 76 and as *c.* 44 for the fractured gneiss, demonstrating a more accurate representation of the rock  
366 mass strength differences of the massive and fractured gneiss.

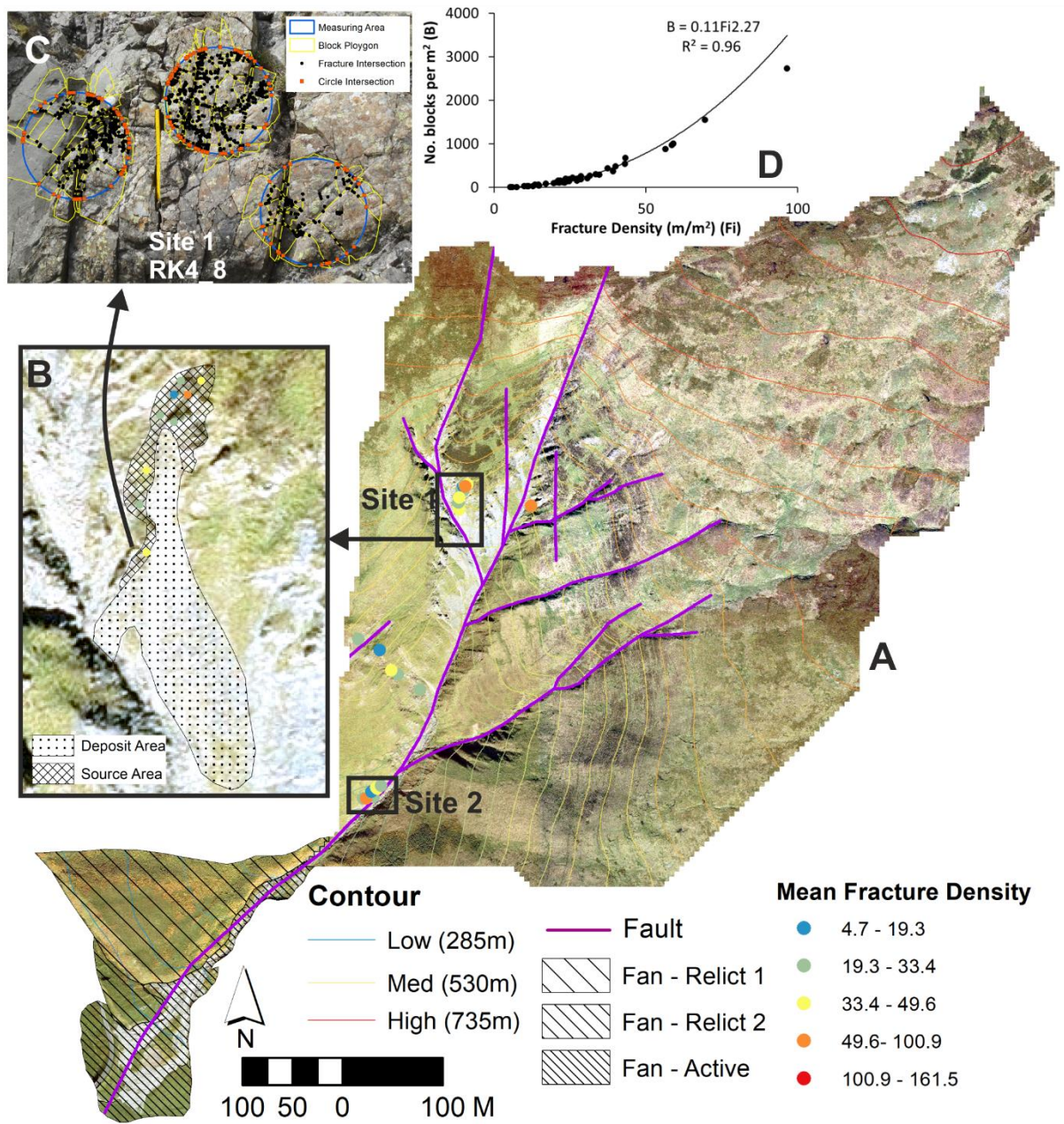
367

### 368 **4.3 Block size and rock erodibility, Codleteith Burn catchment, Southern Scotland**

369 Geohazards related to active geomorphic processes such as debris flows and landslides affect many  
370 upland areas. Pre-existing fractures are a significant factor in the preconditioning of rock masses for  
371 erosion at the Earth’s surface (e.g. Clarke and Burbank, 2010; Dühnforth et al. 2010; Roy *et al.* 2016).  
372 Areas of intensely fractured rocks are thus more likely to be associated with higher susceptibility to  
373 debris flow and landslide hazards. This susceptibility is likely to be driven both by higher volumes of  
374 material being produced from hillslopes underlain by highly fractured rocks, and by the size distribution  
375 of sediment grains entering the geomorphic systems (e.g. Sklar *et al.* 2016). To understand the controls  
376 exerted by the rock mass properties on geomorphic systems, the spatial variability in fracture networks  
377 in bedrock needs to be adequately characterised at catchment scales. This characterisation is challenging  
378 in many upland settings as high spatial variability means that large data sets from multiple sites are  
379 required, yet practical difficulties accessing sites are common in steep terrain.

380 The 2D fracture digitisation method is here used to assess the spatial distribution of block-size and  
381 fracture density of metasandstone of low metamorphic grade in the Southern Uplands, southern  
382 Scotland (Figure 5). The use of the 2D digital method allowed for a nested sampling approach, to  
383 characterise variability across a range of length scales, from meter (Figure 5C), to decimetre (Figure  
384 5B), to catchment (Figure 5A). Block density can be expressed as blocks per square metre, which is

385 easily derived from a polygonised set of fracture traces, and is related to the fracture density (Figure  
 386 5D). Whether this 2D block size measure is representative for the true 3D block size depends on the  
 387 anisotropy of the fracture system and the average block shape. Despite consistent bedrock type  
 388 (metasandstone) across the study area, fault-related fracturing gives rise to highly variable fracture  
 389 density across the study area, and variations in 2D block size estimates from <50 to >1000 blocks per  
 390 m<sup>2</sup> (Figure 5D). These data help to quantify the way in which rock mass parameters such as fracture  
 391 density influence key geomorphic process elements such as block size. This type of data can be used to  
 392 inform modelling of erosion and sediment movement within landscapes.



393

394 **Figure 5.** Multi-scalar fracture network and block-size analysis for the Codleteith Burn catchment in the Southern  
 395 Uplands of Scotland (A). Sites 1 (B) and 2 (not shown) are sub-catchment hillslope source areas sampled at high

396 resolution. Variability at the outcrop-scale was captured using multiple sampling windows per image (C). The  
397 number of blocks sampled per m<sup>2</sup> is strongly related to the fracture density (D).

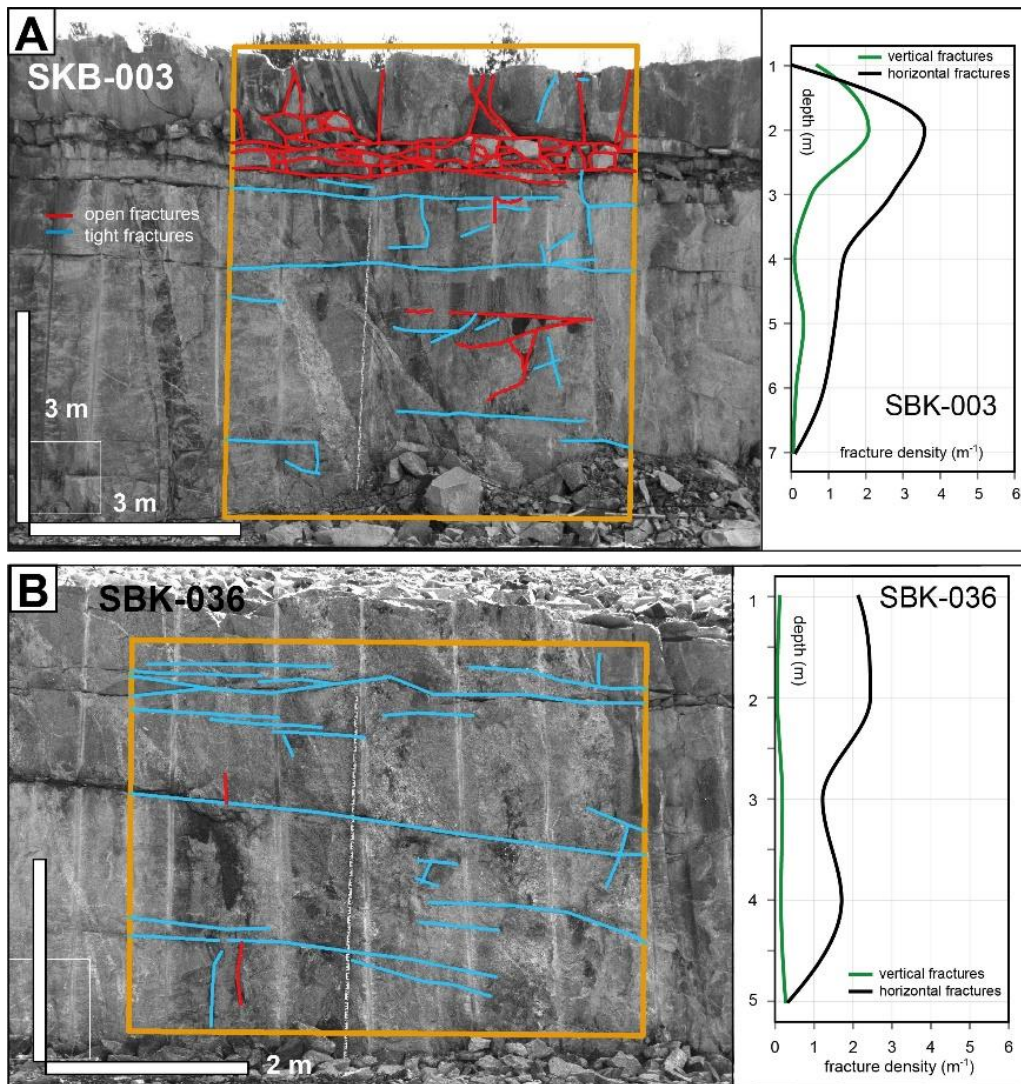
398

#### 399 **4.4 Application to historic photographs of shallow basement fractures, eastern Sweden.**

400 During the construction of the Forsmark nuclear power plant in east Sweden in the 1970s, a series of  
401 excavations for shafts, tunnels and cooling water canals were dug out in basement gneiss rocks. In these  
402 excavations, numerous subhorizontal fractures were encountered, many of which were dilated and filled  
403 with water-lain silt and sand. Many aspects of this shallow fracture network were documented at the  
404 time, including aperture and roughness, density, orientation, coatings (chlorite, epidote etc), as well as  
405 a characterisation of the sediment fills (Stephansson and Ericsson, 1975; Carlsson and Olsson, 1976;  
406 Carlsson 1979). As construction was completed the excavations were graded, or concreted over or  
407 filled with water and are not available for study anymore. The shallow fracture network remained of  
408 interest to establish the potential of groundwater overpressure and hydraulic jacking of basement  
409 fractures (e.g. Pusch *et al.* 1990; Talbot 1990; Lönnqvist and Hökmark, 2013; Talbot, 2014), as well as  
410 playing a potentially important role in a newly recognised erosion mechanism, termed glacial ripping  
411 (Hall *et al.* 2020). For this latter (ongoing) research one relevant issue is the fracture density of  
412 subvertical and subhorizontal fractures as a function of depth in sections with and without fracture  
413 dilation: data that was not gathered during the original studies in the 1970s.

414 To acquire this data, high quality historic photos were used. All photographs contain a clearly  
415 recognisable measuring stick, and could thus be georeferenced accurately. Digitisation followed the  
416 methods described in this paper. Fracture aperture characteristics were attributed to the digital traces  
417 based on their appearance in the photographs. The shapefile of fracture traces was imported into python,  
418 with which spatial parameters such as orientation were calculated and fractures were separated into  
419 subhorizontal and subvertical attitudes. Total fracture trace length was calculated for each 1 m depth  
420 interval and fracture density for each interval was subsequently calculated. The results are plotted as a  
421 density-depth profile, and a cubic interpolation was used to smooth the curve (Figure 6). Results show  
422 a clear difference in fracture density between different sections (Figure 6A, B). A further difference is  
423 that in some sections (e.g. SKB-003) both the subvertical and subhorizontal fracture densities increase  
424 towards rockhead, whilst in other sections (SKB-036) only the subhorizontal fracture density show a  
425 marked increase.

426



427

428 **Figure 6.** 2D fracture analysis applied to historic photographs of excavations during the construction of the  
 429 Forsmark nuclear power plant, eastern Sweden. Photos: Göran Hansson. Open and tight fractures (red/blue)  
 430 were digitised. Fracture density was calculated separately for subvertical and horizontal fractures.

431

## 432 5 Discussion

### 433 5.1 Overview of case studies

434 The case studies presented here highlight a range of benefits from the use of the 2D digital method for  
 435 different applications. The Cauvery Catchment case study demonstrates how 2D digital capture  
 436 provided flexibility to gather data for estimation of regional aquifer properties on a short  
 437 reconnaissance-style field-campaign, with fracture data collected retrospectively from photographs  
 438 taken at key localities. The 2D digital dataset allows for evolved quantitative and graphical data  
 439 analysis, such as heat maps of fracture intersections to better understand connectivity. For engineering  
 440 geology purposes, commonly-used qualitative approaches for estimating key rock mass strength  
 441 parameters such as the geological strength index (GSI) are subject to variability through interpretation

442 bias and practitioner experience, resulting in increased uncertainty, and potentially in higher project  
443 risks and costs. In the case study presented here, the 2D digital method is shown to provide a more  
444 accurate and consistent representation of the geological strength index (GSI) of a rock mass than the  
445 commonly-used qualitative estimators (e.g. Hoek, 1983; Sönmez and Ulusay, 1999). In geomorphic  
446 studies, quantitative characterisation of rock mass strength is increasingly important for  
447 parameterisation of process and landscape-evolution models (e.g. Roy *et al.* 2016; Sklar *et al.* 2017).  
448 The Codleteith Burn Catchment study demonstrates the potential of the 2D digital method for multi-  
449 scalar fracture analysis in challenging terrain. In eastern Sweden, the historic photographs were the  
450 best source for capturing specific fracture parameters in the shallow basement, and the 2D digital  
451 method is the only possible way to retrospectively gather this data.

452 A number of modern applied geoscience studies, such as in groundwater modelling (Babadagli, 2001),  
453 geothermal energy (Hitchmough *et al.*, 2007) and geotechnical engineering (Bandpey *et al.*, 2019) use  
454 field-based-only methods to gather fracture network data. Field measurements of geometry and density  
455 of fractures networks are used to understand the mechanical and hydraulic properties of a rock mass  
456 (Babadagli, 2001; Maréchal *et al.* 2004; Siddique *et al.* 2015). The 2D digital method described would  
457 be ideally suited to such case studies to improve the quality of data collected and allowing for more  
458 advanced analysis. In these studies, field time and accessibility of the outcrop are a major consideration  
459 for the type and amount of fracture data collected. When time is limited a 1D method is used to collect  
460 fracture data (Bandpey *et al.* 2017), whereas the new digital method would allow full 2D fracture traces  
461 to be collected efficiently. In studies that look at slope stability on narrow mountain roads in the  
462 Himalayas (Siddique *et al.*, 2015), limited fracture data is used in rock quality calculations, which is  
463 likely due a combination of time constrains and the inaccessibility of the outcrop. The digital method  
464 would provide a more accurate estimate of fracture geometries when modelling slope processes (e.g.  
465 Pradhan and Siddique, 2020).

## 466 **5.2 Benefits and limitations**

467 The capture and publication of digital objects such as digital fracture network traces and derived  
468 parameters is an increasingly valuable part of the geoscience research process, facilitating evaluation  
469 and supporting ongoing scientific discovery (Gil *et al.* 2016). The case studies demonstrate that the 2D  
470 digital method described herein represents a valuable tool for analysing fracture networks, facilitating  
471 the efficient capture of quantitative datasets through a systematic and reproducible approach.  
472 Nevertheless, there are benefits and limitations compared to other fracture capture methods.

473 The 2D digital method is as rapid, if not more so, than a 1D scan-line survey. However, the 2D digital  
474 method does not capture the direct field observations such as orientation, roughness, aperture and any  
475 secondary fills. These parameters are useful for understanding rock mass strength or permeability  
476 (Carlsson, 1979; Laubach *et al.* 2019). If such direct observational data are required for the study (and

477 practical on the outcrop in question), it is perfectly possible to first perform the 2D digital fracture  
478 capture as described herein, and then return to the study site and augment the dataset with further  
479 observational data as attributes; portable PC tablets are ideal for this purpose.

480 A major drawback of the 2D digital method is that it captures the fractures that are at a high angle to  
481 the outcrop plane, but not those that are subparallel to it. It is these fractures that will be particularly  
482 important for slope stability studies. This can be mitigated by analysing outcrop faces at different angles,  
483 but this may not always be possible. In these cases, an additional scan-line survey, focusing on fracture  
484 orientations, may be added to the study, or – if resources allow – a 3D scanning survey could be  
485 undertaken. The 3D scanning method does gather more data, including orientation of exposed fracture  
486 surfaces. This method is probably preferred for intense, localised studies, such as local, high-value  
487 infrastructure projects, or other key sites. However, 3D scanning methods are resource intensive, and  
488 likely not cost-effective if a fracture network analysis of multiple sites across a region is required, for  
489 instance for long infrastructure projects or regional groundwater studies.

490 Finally, the 2D digital method is the only method to capture data from historic images, valuable for the  
491 retrospective analysis of temporary sections during construction or quarrying, which can be crucial if  
492 existing exposure is limited.

## 493 **6 Conclusions**

494 The aim of this paper is to describe, evaluate and develop a simple but robust, low-cost method for  
495 capturing 2D fracture network data in GIS, and make it more accessible to a broader range of users in  
496 both academia and industry. We present a breakdown of the key steps in the methodology, which  
497 provides an understanding of how to avoid error and improve the accuracy of the final dataset. The 2D  
498 digital method can be used to interpret traces of 2D linear features of a wide variety of scales from the  
499 outcrop scale to the regional-scale, using outcrop photos, aerial photographs, DEMs or satellite imagery.

500 An important aspect of applied geosciences is the use of fracture network parameters to characterise a  
501 rock mass in terms of rock mass strength and fluid flow properties. The field-based methodology for  
502 determining fracture network parameters can be time consuming and impractical, when field time is  
503 limited or outcrops are inaccessible. 2D digital fracture trace capture is an accurate and rapid method  
504 of quantifying 2D linear networks using open access software packages. It offers a robust, cost-effective  
505 methodology that can be used in academia and industry to gather accurate 2D fracture network data. The  
506 low-cost nature of the method means that it can be applied to a large number of outcrops, so that in  
507 studies where the spatial variability of fracture networks is important, large datasets can be generated  
508 cost effectively. Systematic capture and publication of 2D digital fracture datasets has significant  
509 potential to enhance future geoscience research by making aggregated analysis (meta-analysis) possible.

510

511 **Acknowledgements**

512 This paper was supported by the British Geological Survey NC-ODA grant NE/R000069/1: *Geoscience*  
513 *for Sustainable Futures* and is published with the permission of the Executive Director of the Geological  
514 Survey. Assen Simeonov from SKB (Swedish Nuclear Fuel and Waste Management Co), is thanked  
515 for sourcing the historic photos of the Forsmark construction. Martin Gillespie is thanked for helpful  
516 comments on the manuscript. The paper has benefited from detailed comments from Francesco  
517 Mazzarini and two anonymous reviewers.

518

519 **References**

- 520 Babadagli, T.: Fractal analysis of 2-D fracture networks of geothermal reservoirs in south-western  
521 Turkey, *Journal of volcanology and geothermal research*, 112, 83-103, 2001.
- 522 Bandpey, A. K., Shahriar, K., Sharifzadeh, M., and Marefvand, P.: Comparison of methods for  
523 calculating geometrical characteristics of discontinuities in a cavern of the Rudbar Lorestan  
524 power plant, *Bulletin of Engineering Geology and the Environment*, 1-21, 2017.
- 525 Bandpey, A. K., Shahriar, K., Sharifzadeh, M., and Marefvand, P.: Comparison of methods for  
526 calculating geometrical characteristics of discontinuities in a cavern of the Rudbar Lorestan  
527 power plant, *Bulletin of Engineering Geology and the Environment*, 78, 1073-1093, 2019.
- 528 Barton, N., Lien, R., and Lunde, J.: Engineering classification of rock masses for the design of tunnel  
529 support, *Rock mechanics*, 6, 189-236, 1974.
- 530 Bisdom, K., Nick, H., and Bertotti, G.: An integrated workflow for stress and flow modelling using  
531 outcrop-derived discrete fracture networks, *Computers & Geosciences*, 103, 21-35, 2017.
- 532 Carlsson, A: Characteristic Features of a Superficial Rock Mass in Southern Sweden (doct. thesis),  
533 1979.
- 534 Carlsson, A., and Olsson, T.: Joint fillings at Forsmark, Uppland, Sweden: A discussion, *Geologiska*  
535 *Föreningen i Stockholm Förhandlingar*, 98, 75-77, 1976.
- 536 Clarke, B. A., and Burbank, D. W.: Bedrock fracturing, threshold hillslopes, and limits to the magnitude  
537 of bedrock landslides, *Earth and Planetary Science Letters*, 297, 577-586, 2010.
- 538 Collins, S. L., Loveless, S. E., Muddu, S., Buvaneshwari, S., Palamakumbura, R. N., Krabbendam, M.,  
539 Lapworth, D. J., Jackson, C. R., Goody, D. C., and Nara, S. N. V.: Groundwater connectivity  
540 of a sheared gneiss aquifer in the Cauvery River basin, India, *Hydrogeology Journal*, 2020.
- 541 Davis, G. H., Reynolds, S. J., and Kluth, C. F.: *Structural geology of rocks and regions*, John Wiley &  
542 Sons, 2011.
- 543 Dühnforth, M., Anderson, R. S., Ward, D., and Stock, G. M.: Bedrock fracture control of glacial erosion  
544 processes and rates, *Geology*, 38, 423-426, 2010.

545 Follin, S., Hartley, L., Rhén, I., Jackson, P., Joyce, S., Roberts, D., and Swift, B.: A methodology to  
546 constrain the parameters of a hydrogeological discrete fracture network model for sparsely  
547 fractured crystalline rock, exemplified by data from the proposed high-level nuclear waste  
548 repository site at Forsmark, Sweden, *Hydrogeology Journal*, 22, 313-331, 2014.

549 Gao, M., Xu, X., Klinger, Y., van der Woerd, J., and Tapponnier, P.: High-resolution mapping based  
550 on an Unmanned Aerial Vehicle (UAV) to capture paleoseismic offsets along the Altyn-Tagh  
551 fault, China, *Scientific Reports*, 7, 1-11, 2017.

552 Gil, Y., David, C. H., Demir, I., Essawy, B. T., Fulweiler, R. W., Goodall, J. L., Karlstrom, L., Lee, H.,  
553 Mills, H. J., Oh, J-H, Pierce, S. A., Pope, A., Tzeng, M. W., Villamizar, S. R., Yu, X.: Toward  
554 the Geoscience Paper of the Futures: Best practises for documenting and sharing research from  
555 data to software to provenance, *Earth and Space Science*, 3, 388-415.

556 Gillespie, P., Johnston, J., Loriga, M., McCaffrey, K., Walsh, J., and Watterson, J.: Influence of layering  
557 on vein systematics in line samples, Geological Society, London, *Special Publications*, 155, 35-  
558 56, 1999.

559 Guihéneuf, N., Boisson, A., Bour, O., Dewandel, B., Perrin, J., Dausse, A., Viossanges, M., Chandra,  
560 S., Ahmed, S., and Maréchal, J.: Groundwater flows in weathered crystalline rocks: Impact of  
561 piezometric variations and depth-dependent fracture connectivity, *Journal of Hydrology*, 511,  
562 320-334, 2014.

563 Hall, A. M., Krabbendam, M., van Boeckel, M., Goodfellow, B. W., Hättestrand, C., Heyman, J.,  
564 Palamakumbura, R., Stroeven, A. P., and Näslund, J.-O.: Glacial ripping: geomorphological  
565 evidence from Sweden for a new process of glacial erosion, *Geografiska Annaler: Series A,*  
566 *Physical Geography*, 2020.

567 Hancock, P.: Brittle microtectonics: principles and practice, *Journal of structural geology*, 7, 437-457,  
568 1985.

569 Hardebol, N., and Bertotti, G.: DigiFract: A software and data model implementation for flexible  
570 acquisition and processing of fracture data from outcrops, *Computers & Geosciences*, 54, 326-  
571 336, 2013.

572 Healy, D., Rizzo, R. E., Cornwell, D. G., Farrell, N. J., Watkins, H., Timms, N. E., Gomez-Rivas, E.,  
573 and Smith, M.: FracPaQ: A MATLAB™ toolbox for the quantification of fracture patterns,  
574 *Journal of Structural Geology*, 95, 1-16, 2017.

575 Hitchmough, A. M., Riley, M. S., Herbert, A. W., and Tellam, J. H.: Estimating the hydraulic properties  
576 of the fracture network in a sandstone aquifer, *Journal of contaminant hydrology*, 93, 38-57,  
577 2007.

578 Hoek, E.: Strength of jointed rock masses, *Geotechnique*, 33, 187-223, 1983.

579 Hoek, E., and Brown, E. T.: Practical estimates of rock mass strength, *International journal of rock*  
580 *mechanics and mining sciences*, 34, 1165-1186, 1997.

581 Krabbendam, M., and Glasser, N. F.: Glacial erosion and bedrock properties in NW Scotland: abrasion  
582 and plucking, hardness and joint spacing, *Geomorphology*, 130, 374-383, 2011.

583 Krabbendam, M., and Bradwell, T.: Quaternary evolution of glaciated gneiss terrains: pre-glacial  
584 weathering vs. glacial erosion, *Quaternary Science Reviews*, 95, 20-42, 2014.

585 Krabbendam, M., Eyles, N., Putkinen, N., Bradwell, T., and Arbelaez-Moreno, L.: Streamlined hard  
586 beds formed by palaeo-ice streams: A review, *Sedimentary Geology*, 338, 24-50, 2016.

587 Laubach, S. E., Lander, R., Criscenti, L. J., Anovitz, L. M., Urai, J., Pollyea, R., Hooker, J. N., Narr,  
588 W., Evans, M. A., and Kerisit, S. N.: The role of chemistry in fracture pattern development and  
589 opportunities to advance interpretations of geological materials, *Reviews of Geophysics*, 57,  
590 1065-1111, 2019.

591 Liu, Y.-C., and Chen, C.-S.: A new approach for application of rock mass classification on rock slope  
592 stability assessment, *Engineering geology*, 89, 129-143, 2007.

593 Long, J. C., and Billaux, D. M.: From field data to fracture network modeling: an example  
594 incorporating spatial structure, *Water resources research*, 23, 1201-1216, 1987.

595 Lönnqvist, M., and Hökmark, H.: Approach to estimating the maximum depth for glacially induced  
596 hydraulic jacking in fractured crystalline rock at Forsmark, Sweden, *Journal of Geophysical  
597 Research: Earth Surface*, 118, 1777-1791, 2013.

598 Manzocchi, T.: The connectivity of two-dimensional networks of spatially correlated fractures, *Water  
599 Resources Research*, 38, 1-1-1-20, 2002.

600 Maréchal, J.-C., Dewandel, B., and Subrahmanyam, K.: Use of hydraulic tests at different scales to  
601 characterize fracture network properties in the weathered-fractured layer of a hard rock aquifer,  
602 *Water Resources Research*, 40, 2004.

603 Maréchal, J.-C., Dewandel, B., Ahmed, S., Galeazzi, L., and Zaidi, F. K.: Combined estimation of  
604 specific yield and natural recharge in a semi-arid groundwater basin with irrigated agriculture,  
605 *Journal of Hydrology*, 329, 281-293, 2006.

606 Marinos, P., and Hoek, E.: GSI: a geologically friendly tool for rock mass strength estimation, *ISRM  
607 international symposium*, 2000,

608 Mauldon, M., Dunne, W., and Rohrbaugh Jr, M.: Circular scanlines and circular windows: new tools  
609 for characterizing the geometry of fracture traces, *Journal of Structural Geology*, 23, 247-258,  
610 2001.

611 McCaffrey, K., Holdsworth, R., Pless, J., Franklin, B., and Hardman, K.: Basement reservoir  
612 plumbing: fracture aperture, length and topology analysis of the Lewisian Complex, NW  
613 Scotland, *Journal of the Geological Society*, 2020.

614 Menegoni, N., Giordan, D., Perotti, C., and Tannant, D. D.: Detection and geometric characterization  
615 of rock mass discontinuities using a 3D high-resolution digital outcrop model generated from  
616 RPAS imagery—Ormea rock slope, Italy, *Engineering geology*, 252, 145-163, 2019.

617 Müller, L.: *Rock mechanics*, Springer, 1974.

618 Nyberg, B., Nixon, C. W., and Sanderson, D. J.: NetworkGT: A GIS tool for geometric and topological  
619 analysis of two-dimensional fracture networks, *Geosphere*, 14, 1618-1634, 2018.

620 Odling, N., Gillespie, P., Bourguine, B., Castaing, C., Chiles, J., Christensen, N., Fillion, E., Genter, A.,  
621 Olsen, C., and Thrane, L.: Variations in fracture system geometry and their implications for fluid  
622 flow in fractures hydrocarbon reservoirs, *Petroleum Geoscience*, 5, 373-384, 1999.

623 Panthee, S., Singh, P., Kainthola, A., and Singh, T.: Control of rock joint parameters on deformation of  
624 tunnel opening, *Journal of Rock Mechanics and Geotechnical Engineering*, 8, 489-498, 2016.

625 Park, H.-J., West, T. R., and Woo, I.: Probabilistic analysis of rock slope stability and random properties  
626 of discontinuity parameters, Interstate Highway 40, Western North Carolina, USA, *Engineering  
627 Geology*, 79, 230-250, 2005.

628 Perrin, J., Ahmed, S., and Hunkeler, D.: The effects of geological heterogeneities and piezometric  
629 fluctuations on groundwater flow and chemistry in a hard-rock aquifer, southern India,  
630 *Hydrogeology Journal*, 19, 1189, 2011.

631 Pless, J.: Characterising fractured basement using the Lewisian Gneiss Complex, NW Scotland:  
632 implications for fracture systems in the Clair Field basement, Durham University, 2012.

633 Pradhan, S. P., and Siddique, T.: Stability assessment of landslide-prone road cut rock slopes in  
634 Himalayan terrain: A finite element method based approach, *Journal of Rock Mechanics and  
635 Geotechnical Engineering*, 12, 59-73, 2020.

636 Procter, A., and Sanderson, D. J.: Spatial and layer-controlled variability in fracture networks, *Journal  
637 of Structural Geology*, 108, 52-65, 2018.

638 Pusch, R., Börgesson, L., and Knutsson, S.: Origin of silty fracture fillings in crystalline bedrock,  
639 *GFF*, 112, 209-213, 1990.

640 Ren, F., Ma, G., Fan, L., Wang, Y., and Zhu, H.: Equivalent discrete fracture networks for modelling  
641 fluid flow in highly fractured rock mass, *Engineering geology*, 229, 21-30, 2017.

642 Rohrbaugh Jr, M., Dunne, W., and Mauldon, M.: Estimating fracture trace intensity, density, and  
643 mean length using circular scan lines and windows, *AAPG bulletin*, 86, 2089-2104, 2002.

644 Roy, S., Tucker, G., Koons, P., Smith, S., and Upton, P.: A fault runs through it: Modeling the influence  
645 of rock strength and grain-size distribution in a fault-damaged landscape, *Journal of Geophysical  
646 Research: Earth Surface*, 121, 1911-1930, 2016.

647 Sanderson, D. J., and Nixon, C. W.: The use of topology in fracture network characterization, *Journal  
648 of Structural Geology*, 72, 55-66, 2015.

649 Sanderson, D. J., and Nixon, C. W.: Topology, connectivity and percolation in fracture networks,  
650 *Journal of Structural Geology*, 115, 167-177, 2018.

651 Schrod, F., Bailey, J.J., Kissling, D.W., Rijdsdijk K.F., Seijmonsbergen A.C., van Ree, D., Hjort, J,  
652 Lawley, R.S., Williams, C.N., Anderson, M.G., Beier, P., van Beukering, P., Boyd, D.S., Brilha,  
653 J., Carcavilla, L., Dahlin, K.M., Gill, J.C., Gordon, J.E., Gray, M., Grundy, M., Hunter, M.L.,  
654 Lawler, J.J., Monge-Ganuzas, M., Royse, K.R., Stewart, I., Record, S., Turner, W., Zarnetske,

655 P.L., and Field, R.: Opinion: To advance sustainable stewardship, we must document not only  
656 biodiversity but geodiversity. *Proceedings of the National Academy of Sciences*, 116 (33) 16155-  
657 16158, 2019.

658 Selby, M. J.: *Hillslope materials and processes*, Hillslope materials and processes., 1982.

659 Senger, K., Buckley, S.J., Chevellier, L., Fagereng, A., Galland, O., Kurz, T.H., Ogata, K., Planke, S.,  
660 and Tve, J.: Fracturing of doleritic intrusions and associated contact zones: Implications for fluid  
661 flow in volcanic basins, *Journal of African Earth Sciences*, 102, 70-85, 2015.

662 Siddique, T., Alam, M. M., Mondal, M., and Vishal, V.: Slope mass rating and kinematic analysis of  
663 slopes along the national highway-58 near Jonk, Rishikesh, India, *Journal of Rock Mechanics  
664 and Geotechnical Engineering*, 7, 600-606, 2015.

665 Singhal, B. B. S., and Gupta, R. P.: *Applied hydrogeology of fractured rocks*, Springer Science &  
666 Business Media, 2010.

667 Sklar, L. S., Riebe, C. S., Marshall, J. A., Genetti, J., Leclere, S., Lukens, C. L., and Merces, V.: The  
668 problem of predicting the size distribution of sediment supplied by hillslopes to rivers,  
669 *Geomorphology*, 277, 31-49, 2017.

670 Sonmez, H., and Ulusay, R.: Modifications to the geological strength index (GSI) and their applicability  
671 to stability of slopes, *International Journal of Rock Mechanics and Mining Sciences*, 36, 743-  
672 760, 1999.

673 Sonmez, H., and Ulusay, R.: A discussion on the Hoek-Brown failure criterion and suggested  
674 modifications to the criterion verified by slope stability case studies, *Yerbilimleri*, 26, 77-99,  
675 2002.

676 Stephansson, O., and Ericsson, B.: Pre-Holocene joint fillings at Forsmark, Uppland, Sweden,  
677 *Geologiska Föreningen i Stockholm Förhandlingar*, 97, 91-95, 1975.

678 Stober, I., and Bucher, K.: Hydraulic properties of the crystalline basement, *Hydrogeology Journal*, 15,  
679 213-224, 2007.

680 Strijker, G., Bertotti, G., and Luthi, S. M.: Multi-scale fracture network analysis from an outcrop  
681 analogue: A case study from the Cambro-Ordovician clastic succession in Petra, Jordan, *Marine  
682 and Petroleum Geology*, 38, 104-116, 2012.

683 Talbot, C.: Problems posed to a bedrock radwaste repository by gently dipping fracture zones,  
684 *Geologiska Föreningen i Stockholm Förhandlingar*, 112, 355-359, 1990.

685 Talbot, C. J.: Comment on “Approach to estimating the maximum depth for glacially induced  
686 hydraulic jacking in fractured crystalline rock at Forsmark, Sweden” by M. Lönnqvist and H.  
687 Hökmark, *Journal of Geophysical Research: Earth Surface*, 119, 951-954, 2014.

688

689 Tavani, S., Corradetti, A., and Billi, A.: High precision analysis of an embryonic extensional fault-  
690 related fold using 3D orthorectified virtual outcrops: The viewpoint importance in structural  
691 geology, *Journal of Structural Geology*, 86, 200-210, 2016.

692 Ukar, E., Laubach, S. E., and Hooker, J. N.: Outcrops as guides to subsurface natural fractures: Example  
693 from the Nikanassin Formation tight-gas sandstone, Grande Cache, Alberta foothills, Canada,  
694 *Marine and Petroleum Geology*, 103, 255-275, 2019.

695 Vasuki, Y., Holden, E.-J., Kovesi, P., and Micklethwaite, S.: Semi-automatic mapping of geological  
696 Structures using UAV-based photogrammetric data: An image analysis approach, *Computers &  
697 Geosciences*, 69, 22-32, 2014.

698 Voorn, M., Exner, U., Barnhoorn, A., Baud, P., and Reuschlé, T.: Porosity, permeability and 3D fracture  
699 network characterisation of dolomite reservoir rock samples, *Journal of Petroleum Science and  
700 Engineering*, 127, 270-285, 2015.

701 Watkins, H., Bond, C. E., Healy, D., and Butler, R. W.: Appraisal of fracture sampling methods and a  
702 new workflow to characterise heterogeneous fracture networks at outcrop, *Journal of Structural  
703 Geology*, 72, 67-82, 2015a.

704 Watkins, H., Butler, R. W., Bond, C. E., and Healy, D.: Influence of structural position on fracture  
705 networks in the Torridon Group, Achnashellach fold and thrust belt, NW Scotland, *Journal of  
706 Structural Geology*, 74, 64-80, 2015b.

707 Wüstefeld, P., de Medeiros, M., Koehrer, B., Sibbing, D., Kobbelt, L., and Hilgers, C.: Evaluation of a  
708 workflow to derive terrestrial light detection and ranging fracture statistics of a tight gas  
709 sandstone reservoir analog, *AAPG Bulletin*, 102, 2355-2387, 2018.

710 Zeeb, C., Gomez-Rivas, E., Bons, P. D., and Blum, P.: Evaluation of sampling methods for fracture  
711 network characterization using outcrops, *AAPG bulletin*, 97, 1545-1566, 2013.

712 Zhan, J., Xu, P., Chen, J., Wang, Q., Zhang, W., and Han, X.: Comprehensive characterization and  
713 clustering of orientation data: A case study from the Songta dam site, China, *Engineering  
714 geology*, 225, 3-18, 2017.

715

716

717